SSRG International Journal of Electrical and Electronics Engineering
ISSN: 2348 – 8379 / https://doi.org/10.14445/23488379/IJEEE-V9I8P104

Volume 9 Issue 8, 28-39, August 2022

Original Article

Soft-Switching Integrated Quasi Resonance Buck-Boost Converter for HHO Optimized Grid Connected PV System

Nisha C. Rani[1], N Amuthan[2]

[1]*Department of Electrical and Electronics Engineering, The Oxford College of Engineering, Bangalore, India.*
[2]*Department of Electrical and Electronics Engineering, AMC Engineering College, Bangalore, India.*

[1]*nishashamin@gmail.com*

Received: 18 June 2022 Revised: 13 August 2022 Accepted: 19 August 2022 Published: 31 August 2022

Abstract – *The most economical and ecologically beneficial electrical energy worldwide results from solar photovoltaic systems. However, switching action under normal operation undergoes stress since the voltage or current may not be zero at the changeover time. Here, we suggested the ZVT-ZCT Quasi Resonance Buck-Boost converter (QRBB), which introduces L-C dynamics and induces a forced oscillation, allowing the primary switch (IGBT) to turn off at zero current transition and turn on at zero voltage transition, thereby reducing stress on switching device. Furthermore, the VSI is controlled by the Harris Hawks Optimization Algorithm (HHO) optimized proportional-integral (PI) controller. The proposed dc-dc converter can deliver pure sinusoidal output current and voltage waveforms with better output voltage enhancement. The suggested QRBB Converter's performance and efficiency are tested through simulation using the Matlab Simulink software. The result shows that the PI-HHO controller provides a better steady and dynamic state response and delivers quality power to the grid than the conventional PI controller.*

Keywords – *Global Warming, Solar Photovoltaic Systems, Electrical Energy, Output Voltage, Matlab.*

1. Introduction

Concerns about global warming, the exhaustion of fossil fuels, and technological advancements have made non-conventional energy resources appear as reliable energy sources. Incorporating solar systems into grid-connected systems has increased their significance in today's energy market [7, 15]. The electric power generated from SPV is DC. When we connect SPV to constant frequency grid systems, it takes two stages to complete the energy conversion process ice, DC-DC, and DC-AC conversions are both possible [1]. The energy conversion process for renewable energy systems involves DC-DC buck-boost converters and DC-AC Voltage Source Inverters.

SMPS have become lighter and smaller in the case of a higher switching frequency conversion system. [20] When the switch is a turn on, the current flow will be increased, and the voltage will be decreased across the switch. Now, if there is an overlap between these two transients, this phenomenon is termed hard switching, resulting in switching losses [24]. However, if the switching voltage becomes zero, then the current starts rising. There is theoretically zero turn-on loss. These kinds of switching are known as ‘soft switching’. When we implement resonant components in parallel/series with the switches, the converter can attain zero voltage/current switching for the diode and switch without increasing current and voltage stress. These types of converters are called ZVT/ZCT converters [15]. QSW-ZCS [3] lowers the switch's voltage stress, enables the designer to choose semiconductor devices with a lower voltage rating for the output switch, and eliminates the need for passive RC snubbers, reducing the value of dv/dt, which brings about EMI improvement. [4] The employed ZVT cell in this converter is compatible with high step-up coupled inductor-based boost converters since soft switching is provided by making use of the leakage inductance of coupled inductors in the resonant network. [5] A non-isolated buck converter, resonance and zero voltage transition to achieve zero voltage switching (ZVS) and zero current switching (ZCS) to upgrade the conversion efficiency. [6] SEPIC converter is designed for continuous input current operation.

These auxiliary circuits do, however, work with resonance, which increases the cost and complexity of the circuit. Thus, the soft switching converts reduce the system's efficiency as the auxiliary switches generate the switching losses [8, 9, 13, 17]. As mentioned in [10], the limitations of hard switching in Continuous Conduction Mode are the switching loss due to reverse recovery voltage and higher switching frequency [11]. Despite these limitations, the hard switching methodology has to be modified to reduce or

overcome the effects. Making the voltage or current across the valve zero will make these work properly. [22] A single main switch is used with the suggested system to attain a high gain for QRBB operation. Besides, a capacitor and an inductor are used in the converter to make the ZVT/ZCT for the main IGBT switch to obtain the soft switching.

The main objectives of such systems are reducing the converter's frequency deviation, assuring system dependability, and keeping track of the SPV array's maximum output power to raise the grid's energy efficiency.[18] Furthermore, this work introduces a new methodology for PI parameter selection by a dq-vector control scheme, and the HHO algorithm optimizes the parameters. [23]. The effectiveness of the control architecture utilized in the soft-switched QRBB converter connected to a grid inverter is validated using Matlab simulation. This is how the essay is organized. Section 2 presents a summary of the proposed plan. The suggested converter and controller are shown in Section 3. Section 4 presents experimental findings that back up the theoretical idea. Finally, in the last part, the conclusion is addressed.

2. Proposed QRBB Converter with SPV array using ZVT-ZCT

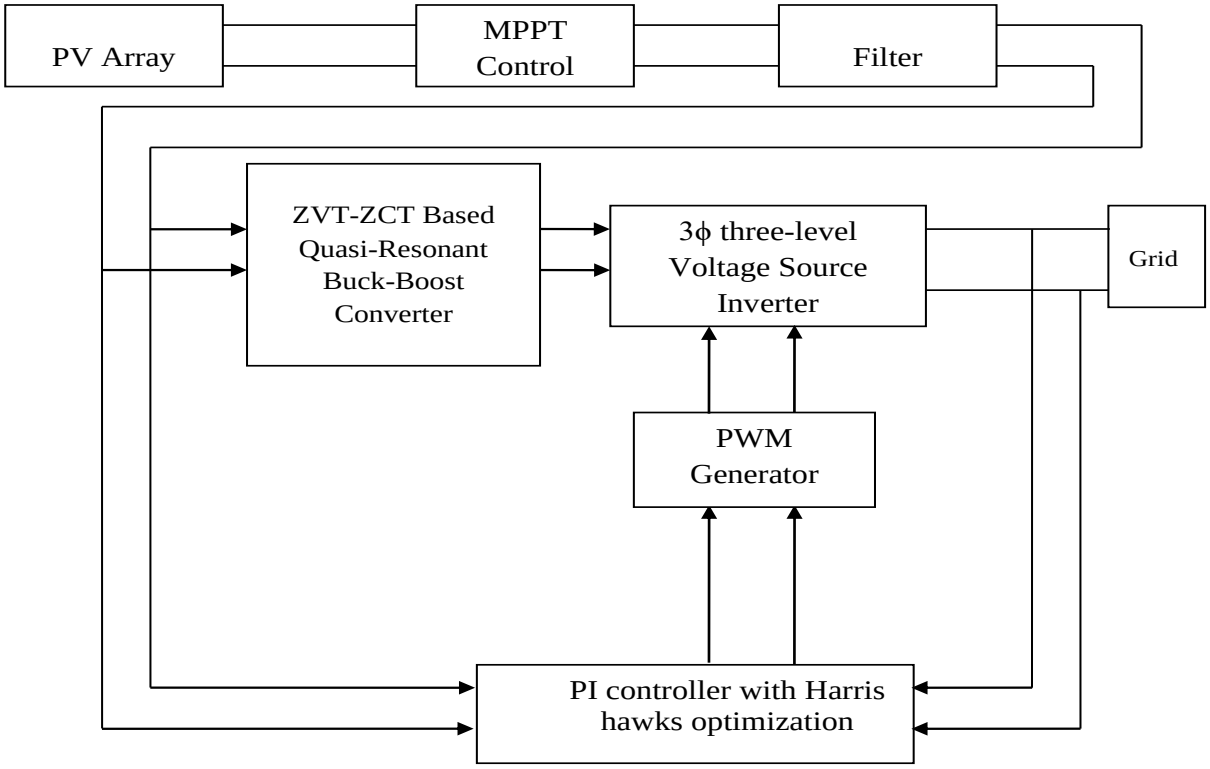

Fig. 1 Block diagram of the Proposed QRBB Converter with SPV array using ZVT-ZCT

Fig. 1 shows a block diagram of an SPV panel connected to a grid using a 3-level Voltage Source Inverter and a ZVT-ZCT Based Quasi-Resonant Buck-Boost Converter (QRBB) (VSI). While the QRBB converter is set to operate in the ZVT/ZCT mode, switching loss is reduced, and the voltage is raised to its maximum level utilizing the Hybrid Incremental Conductance & Integral Regulator technique. To provide the required voltage and optimize power, an MPPT controller regulates the duty cycle (D) of the QRBB converter. The DC connection voltage is converted to AC by the VSI to maintain the power factor at unity. The external loop of the VSI controller increases the DC link voltage, while the controller's internal control loop improves the grid current components Id and Iq. For the external controllers, to maintain unity power factor, a DC voltage regulator sets reference current Iq to zero and outputs reference current Id. Vd and Vq, the present controller's outputs, are converted into the three abc parameters by the PWM generator. The controllers and Phase Lock Loop use a 100 s sample period for their conversion procedure. The PWM generator needs 1 s of sampling time to generate high-resolution waveforms for QRBB and VSI. An array of capacitors filters the harmonics produced by the VSI. The optimization approach. The Harris Hawks Optimization (HHO) technique is used to optimize the PI controller's gain parameters kp, kr.

3. Qualitative Zvs-Zcs Buck-Boost Converter

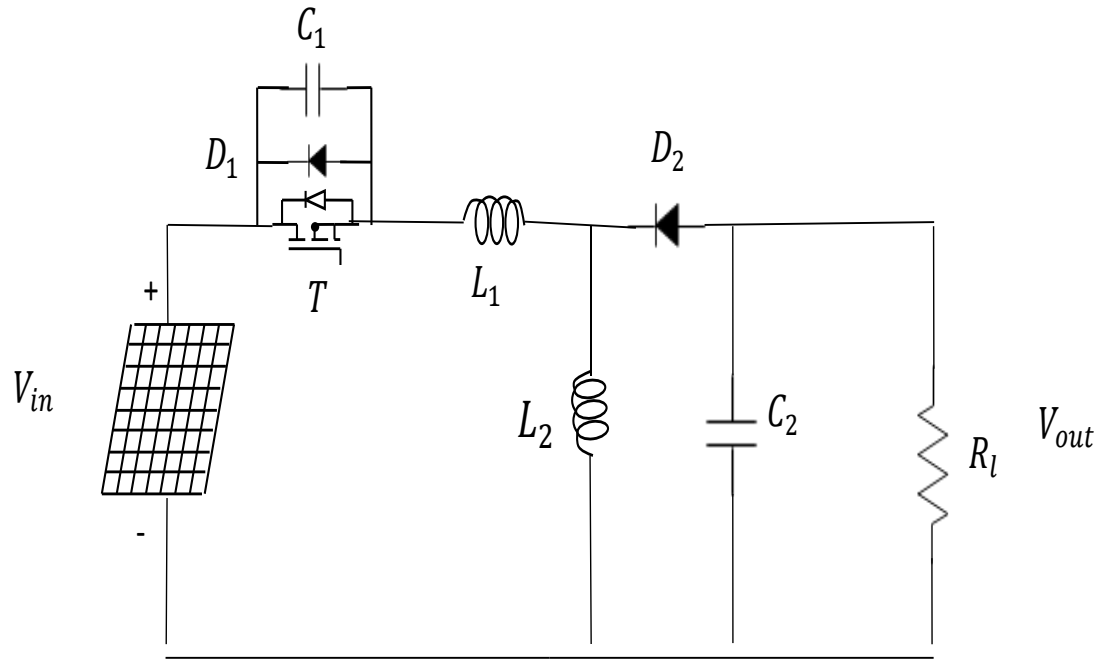

Fig. 2 Proposed auxiliary resonant Buck-Boost converter

Fig. 2 depicts the proposed converter's circuit design. This topology involves two magnetic components (inductor L1 and coupled inductor L2), one MOSFET (T1), two diodes in the first boost stage (D1 and D2), and capacitors C1 and C2 to form a quadruple circuit. The components, inductor L1 and capacitor C1, interact with each other and create an oscillation. Due to this oscillation, the voltage/current across the switch becomes zero at a certain time. Achieving zero voltage/current switching at this precise moment causes the switch's state to change. Fig. 3 shows the quasi-resonant buck-boost converter's steady-state waveforms, which have four operation modes.

3.1. Interval 1: (t = 0)

The IGBT switch and the diode are conducting at the start of Interval 1 (t = 0). Kirchhoff's law can be used to write the voltage equation (1)

$$L_{dt}^{di_L(t)} = V_{in} + V_0 \quad (1)$$

Equation (1) can be solved by integrating both sides with iL(0)=0 as the initial condition. Equation 1 yields iL(t) Equation 2.

$$\boldsymbol{i_L(t) = \frac{V_{in}+V_0}{L} t} \quad (2)$$

$$\boldsymbol{v_{C(t)} = 0} \quad (3)$$

Since the diode must stop conducting when the inductor current hits I_F at time $t=t_3$,t_1 can be expressed using Equation (4)

$$\boldsymbol{t_1 = \frac{LI_F}{V_{in}+V_0}} \quad (4)$$

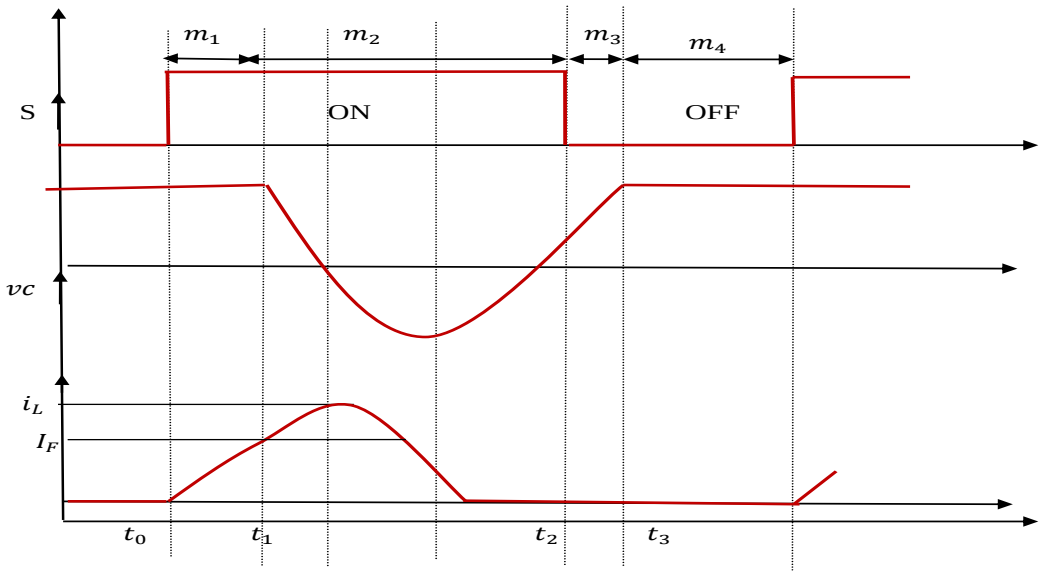

Fig. 3 ZVT buck-boost-based converter steady-state waveform

3.2. Interval 2: ($t_1 \leq t < t_2$)

During this interval, resonance is formed between the inductor and capacitor. The initial conditions are given by Equations 5 and 6,

$$v_C(t_1) = 0 \tag{5}$$

$$i_L(t_1) = I_F \tag{6}$$

By applying Kirchhoff's rule in Fig. 2, the capacitor voltage and inductor current equations can be derived as in Equations 7 and 8.

$$L\frac{di_L}{dt} = V_{in} + V_0 - v_C(t) \tag{7}$$

$$C\frac{dv_C}{dt} = i_L(t) - I_F \tag{8}$$

For $t > t_1$,

$$i_L(t) = I_F + \frac{V_{in}+V_0}{Z_0}\, sin\omega_0(t - t_1) \tag{9}$$

$$v_C(t) = (V_{in} + V_0) + [1 - cos\omega_0(t - t_1)\,] \tag{10}$$

The inductor current hits zero at $t = t_2$ so $i_L(t_2) = 0$, and the switch is turned off. The time interval $(t_2 - t_1)$ is represented by Equation 11.

$$t_2 - t_1) = \frac{1}{\omega_0}\sin^{-1}\left(\frac{I_F Z_0}{V_{in}+V_0}\right) \tag{11}$$

3.3. Interval 3 ($t_3 \leq t < t_4$)

Current across the inductor reaches zero at t=t2. The diode and the IGBT switch are now turned off. At t = t3, When the capacitor approaches zero, it continues to discharge, and at time t=t_3, the diode begins to conduct once more. The current flow through the inductor is zero during this time interval.

$$v_C(t) = \frac{-1}{C}\int_{t_2}^{t} I_F dt = \frac{-I_F}{C}\,(t - t_2) + V_C(t_2) \tag{12}$$

After this phase, the capacitor voltage is zero, t= t3; the diode starts to conduct, which is described in Equation (13),

$$0 = \frac{-I_F}{C}\,(t_3 - t_2) + V_C(t_2) \tag{13}$$

The time between t_2 and t_3 is given in Eq. (14)

$$(t_3 - t_2) = \frac{C}{I_F}V_C(t_2) \tag{14}$$

3.4. Interval 4: ($t_3 \leq t < t_4$)

Between t3 and t4, the diode is switched on after the main switch has been turned off. The switch closes once more after the loop when the current is zero. The modes will be cycled once more

3.5. Voltage Gain

The voltage gain, $M = Vo/Vin$

Eq describes the voltage gain for the ZCS buck-boost converter Equation 16.

$$\frac{M}{1+M} = \frac{f_{ns}}{2\pi}\left[\frac{M}{2Q} + \alpha + \frac{Q}{M}(1 - cos\alpha\right] \tag{15}$$

$$M = \frac{1}{\frac{f_{ns}}{2\pi}\left[\frac{Q}{2M}+\alpha+\frac{M}{Q}(1-cos\alpha\right]} - 1$$

$$\left.\begin{array}{l} M > 0.5\ for\ buck\ opertion \\ M < 2\ for\ boost\ operation \end{array}\right\} \tag{16}$$

In QR-ZVT converters, the primary energy-transfer component is the inductor, while in QR-ZCT converters, it is the capacitor. As a result, current ripples and conduction loss are minimized.

3.6. Design of PI Controller

The control circuit plays a vital role in generating pulses to trigger the switches in the VSI to generate pure sinusoidal waves, high-quality power transferring from the distribution generators to the consumer sections. The system responses of the grid can be improved by properly optimising the controller gains. Harris Hawks Optimization (HHO) algorithm [23] can be approached for optimizing the proportional gain (Kp) and integral gains (Ki) of the PI controller. The external current control loop gives the reference current values given by Equation 17 and Equation 18.

$$i_d^* = (V_{ref} - V)(K_p + \frac{K_i}{s}) \tag{17}$$

$$i_q^* = (f_{ref} - f)(K_p + \frac{K_i}{s}) \tag{18}$$

Also, by utilizing internal current and external voltage loops, the system's dynamic and steady-state response can be improved. Considering reference voltage as the controller output in a synchronously rotating d_q frame, derived by Clarke's transformation and Park's inverse, the resulting voltage reference signals of the controller can be yielded in '$\alpha\ \beta$' axis. PWM technique activates VSI, thereby helping to maintain THD values within limits. Expressions can be given under synchronous dq frame as in Equation 19,

$$\begin{bmatrix} v_d^* \\ v_q^* \end{bmatrix} = \begin{bmatrix} -K_P & -\omega_{LS} \\ \omega_{LS} & -K_P \end{bmatrix} \begin{bmatrix} i_d \\ i_q \end{bmatrix} + \begin{bmatrix} K_P & 0 \\ 0 & K_P \end{bmatrix} \begin{bmatrix} i_d^* \\ i_q^* \end{bmatrix} + \cdots\cdots \begin{bmatrix} K_i & 0 \\ 0 & K_i \end{bmatrix} \begin{bmatrix} X_d \\ X_q \end{bmatrix} \tag{19}$$

Convert Equation 19 into 'abc' frame and '$\alpha\ \beta$' frame by using Clarke's transformations and Park's inverse, respectively,

$$\begin{bmatrix} V_a \\ V_b \\ V_c \end{bmatrix} = \begin{bmatrix} \cos\theta & -\sin\theta & 1 \\ \cos(\theta - \frac{2\pi}{3}) & -\sin(\theta - \frac{2\pi}{3}) & 1 \\ \cos(\theta + \frac{2\pi}{3}) & -\sin(\theta + \frac{2\pi}{3}) & 1 \end{bmatrix} \tag{20}$$

$$\begin{bmatrix} V_\alpha \\ V_\beta \\ V_0 \end{bmatrix} = \frac{2}{3} \begin{bmatrix} V_a \\ V_b \\ V_c \end{bmatrix} \begin{bmatrix} 1 & -1/2 & -1/2 \\ 0 & \sqrt{3}/2 & -\sqrt{3}/2 \\ 1/2 & 1/2 & 1/2 \end{bmatrix} \tag{21}$$

The conventional PI controllers have many limitations, and they cannot set the gain values to a suitable fixed value and automatically regulate the control objectives. Consequently, the predicted values can be attained by optimizing the PI controller with the Harris Hawks Optimization method.

3.7. Harris Hawks Optimization (HHO) Algorithm

The population-based optimization technique known as HHO operates devoid of any patterns. The primary source of inspiration for HHO is the collaborative behavior and "surprise pounce" hunting technique of Harris' hawks in nature. Harris hawks will reveal various team pursuit strategies in light of the complex circumstances and the rabbit's evading behaviors. Fig. 4 illustrates how they wait and then attack in packs with additional hawks approaching from different directions while the rabbit runs in various zigzag patterns.

3.2.1. Phase of Exploration

Two strategies are derived in Equation 22 for Harris' hawks, which perch in random places and wait for prey to be detected.

$$x(t+1) = \begin{cases} Xrand(t) - r1\,|Xrand(t) - 2r2\,X(t)| & q \geq 0.5 \\ \big(Xrabbit(t) - Xm(t)\big) - r3\,\big(LB + r3\,(UB - LB)\big) & q < 0.5 \end{cases} \tag{22}$$

Where $x(t+1)$ denotes the hawk's next iteration position vector, $X(t)$ indicates the hawk's current position vector, $Xrabbit(t)$ denotes the rabbit's position, The random numbers between 0 and 1 are denoted by the letters r1, r2, r3, r4, and r_q. LB refers to lower bounds, and UB refers to upper bounds of variables.

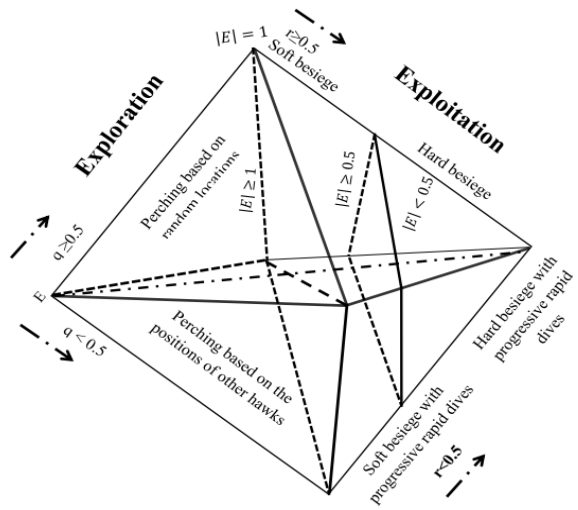

Fig. 4 Different phases of HHO

Equation 23 is used to measure the hawk's average position.

$$Xm(t) = \frac{1}{N} \sum_{i=1}^{N} Xi\,(t) \tag{23}$$

where Xi (t) is the location of each hawk during iteration t. N is the overall hawk number.

3.2.2. Moving from exploration to exploitation

The energy of a rabbit E is designed in terms of its initial state of energy E_0 is described by Equation 24

$$E = 2E_0 (1 - {}^{t}/_{T}) \quad (24)$$

Where T defines the number of iterations.

3.2.3. Exploitation phase

The soft encircling happens when r ≥0.5, and the strong surround happens at |E| ≥ 0.5.

3.2.4. Soft besiege

Soft besiege behavior is modeled by Equation 25 and Equation 26,

$$x(t + 1) = \Delta x(t) - E|JXrabbit(t) - X(t)| \quad (25)$$

$$\Delta x(t) = Xrabbit(t) - X(t) \quad (26)$$

Random jump strength $J = 2(1 - r_5)$

$$X(t + 1) = Xrabbit\,(t) - E|\Delta X(t)| \quad (27)$$

3.2.5. Hard besiege

For Hard encircle, the present positions are mentioned using Equation 27, and the graphical representation of vector addition during hard encircle with prey energy is shown in Fig. 5.

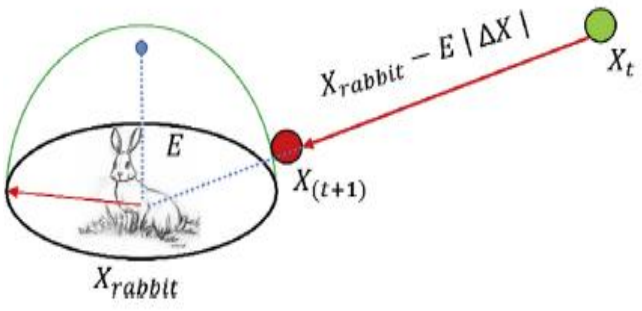

Fig. 5 Vector addition during hard besiege with prey energy

3.2.6. Soft encircle with rapid dives

The rabbit has enough energy to escape the Harris hawk when |E| ≥ 0.5 and r≥ are greater than 0.5.

The hawks can choose to do a mild encircling depending on Equation 28.

$$y = Xrabbit(t) - E|JXrabbit(t) - X(t)| \quad (28)$$

The rabbit will dive by the LF patterns using the rule mentioned in Equation 29.

$$Z = Y + s \times LF(D) \quad (29)$$

The levy flight function is described using Equation 30

$$LF(x) = 0.01 \times \frac{u \times \sigma}{|v|^{\frac{1}{\beta}}} \quad (30)$$

Where, $\beta = 1.5$. As a result, Eq can carry out X (t + 1) of hawks in the soft surround Equation 31.

$$X(t + 1) = \begin{cases} Y & if \;\; F(Y) < F(X(t)) \\ Z & if \;\; F(Z) < F(X(t)) \end{cases} \quad (31)$$

A simple representation of this step for one hawk is explained in Fig. 6.

3.2.7. Hard encircle with rapid dives

When |E| <0.5, before the sudden leap to capture and kill the target, a firm surround is constructed so that the rabbit cannot escape. Less than a gentle surround is the period when the hawks are striving to close the gap between themselves and the escaping prey.

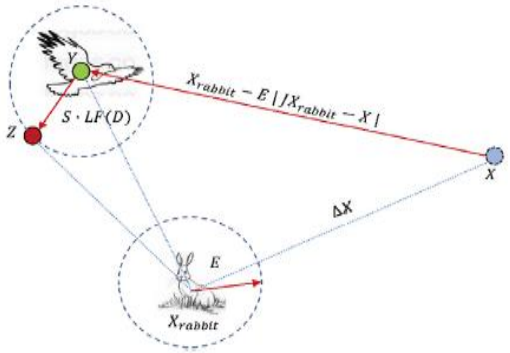

Fig. 6 Overall gentle encircling vectors with quick dips

4. Results and Discussion

The grid-integrated SPV system has been implemented using Matlab/Simulink software. A 100-kW SPV array is linked to a 25-kV grid via a DC-DC ZVT/ZCT QRBB converter and a 3 3-level Voltage Source Inverter (VSI).

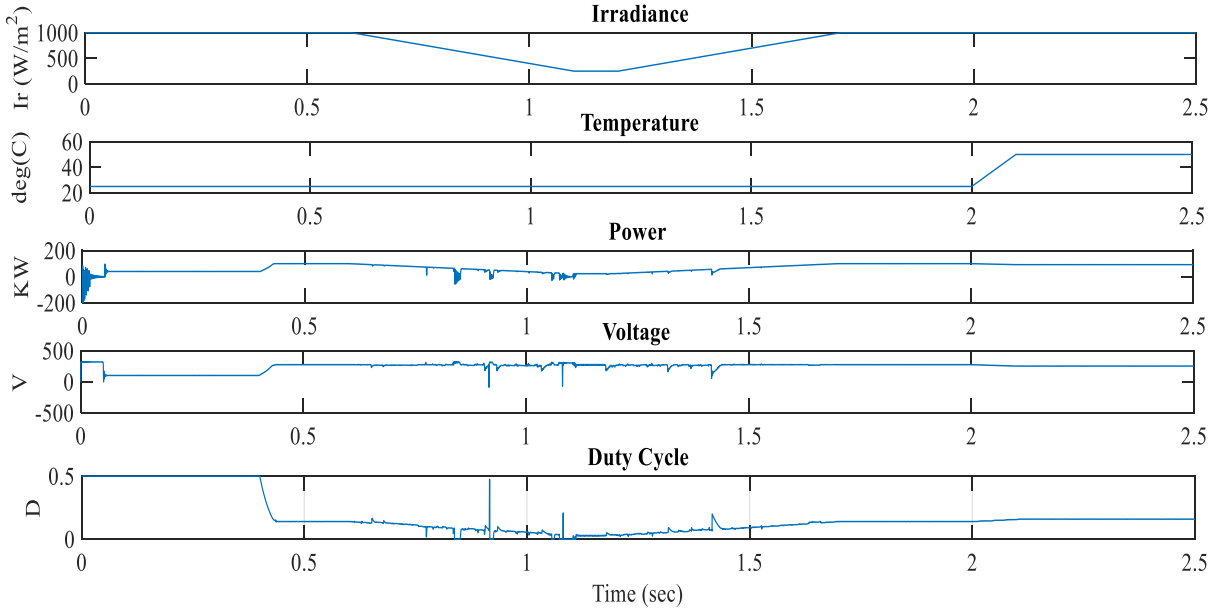

Fig. 7 Output Waveforms of PV Panel

Fig. 7 displays the SPV panel's output power, output voltage, and duty cycle waveforms. At an irradiation level of 1000 W/m2, the solar panel may produce a maximum power of 100 kW. Between t=0.6 and t=1.1, the sun's irradiation decreases from 1000 W/m2 to 250 W/m2. At 1.2 seconds, when the irradiance is reduced to 250 W/m2, the D value is 0.461. The PV voltage is 254 V, and the power is 92.64 kW. The MPPT is still monitoring the maximum power. To study the impact of temperature changes, between t=1.3 and t=2.5 seconds, the sun's brightness increases to 1000 W/m2; at t=2 seconds, the temperature rises to 50 degrees Celsius when the temperature increases from 25°C to 50°C, the output power of the SPV array falls from 100 kW to 93 kW.

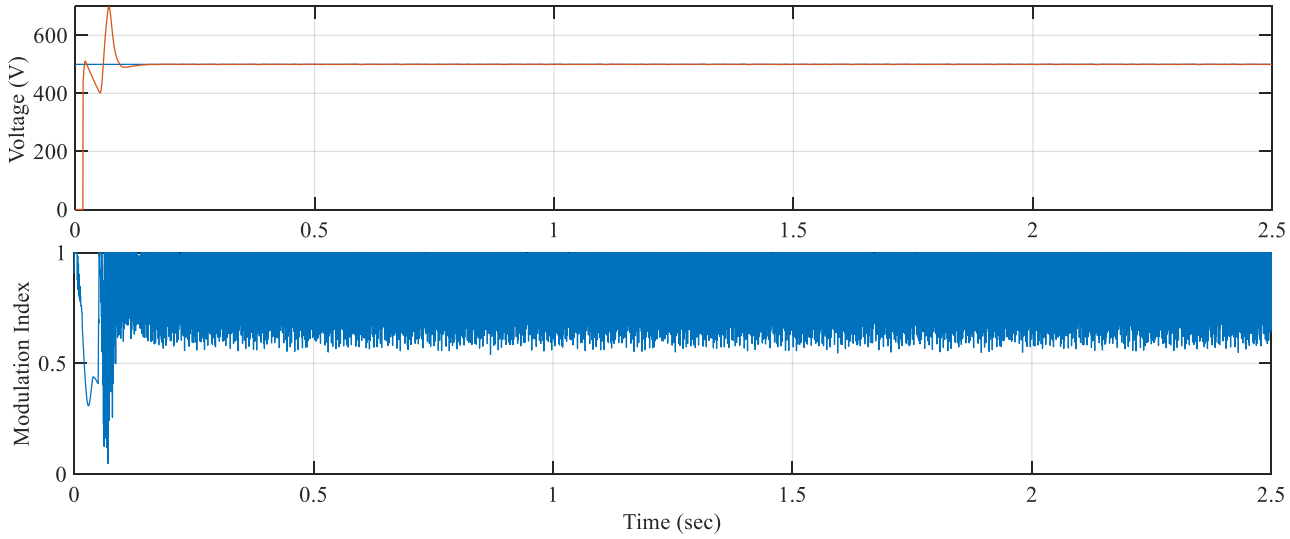

Fig. 8 QRBB Converter's output voltage and its modulation index when using the PI Controller

The PV voltage increases from 254 V DC to 500 V DC using an a5-kHz QRBB converter. The DC-link capacitor is charged to a voltage of over 500 volts and functions as a diode rectifier thanks to the three-level bridge inverter. Fig. 8 shows that the dc reference voltage is constant (500 V), whereas soft switching results in sinusoidal fluctuations of the dc voltage ZVT and ZCT.

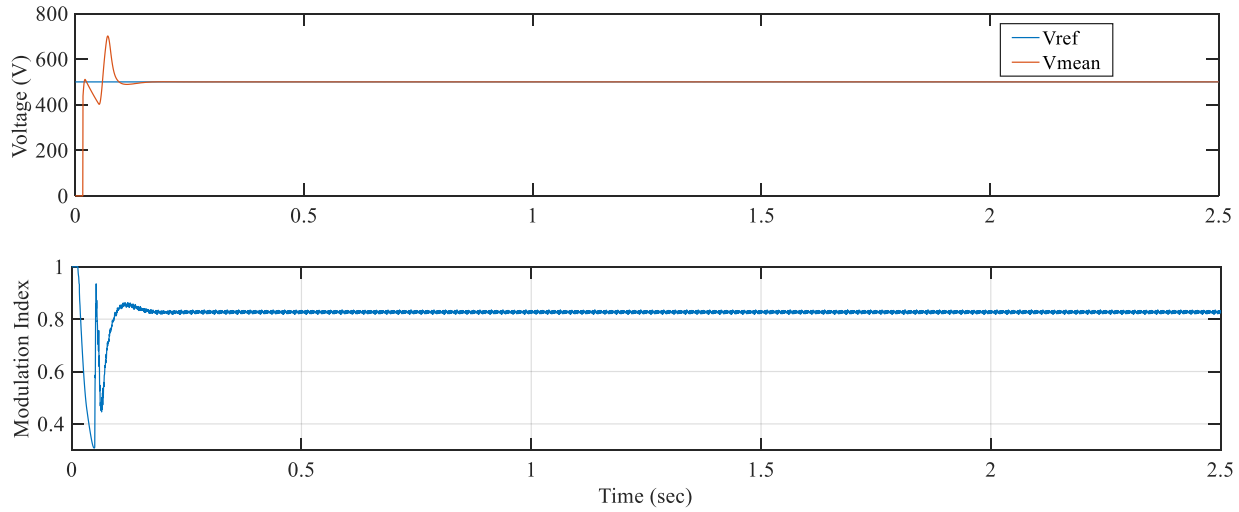

Fig. 9 Output Voltage and Modulation Index of the QRBB Converter with the PI-HHO Controller

During the various periods of the VSI switches, for either ZVT or ZCT situations, the voltage remains zero for a set amount of time. During the voltage oscillation, the Modulation index value varies. Then it remains constant at 0.85 when the oscillations are reduced in the case of using an optimization algorithm observed in Fig. 9.

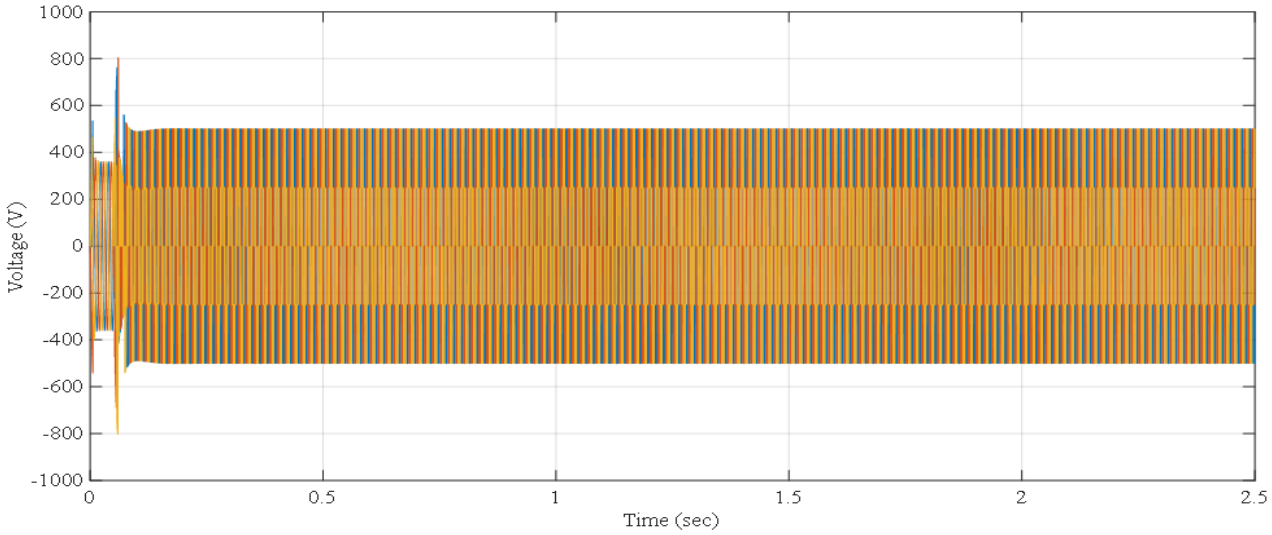

Fig. 10 Output Voltage of VSI with PI controller

As the 500 V DC connection voltage is changed to 260 V AC, the VSI maintains power factor unity, as seen in Fig. 10 and 11. The implementation of soft switching was made possible by using a buck-boost converter and a dc-link VSI with an LC resonant circuit.

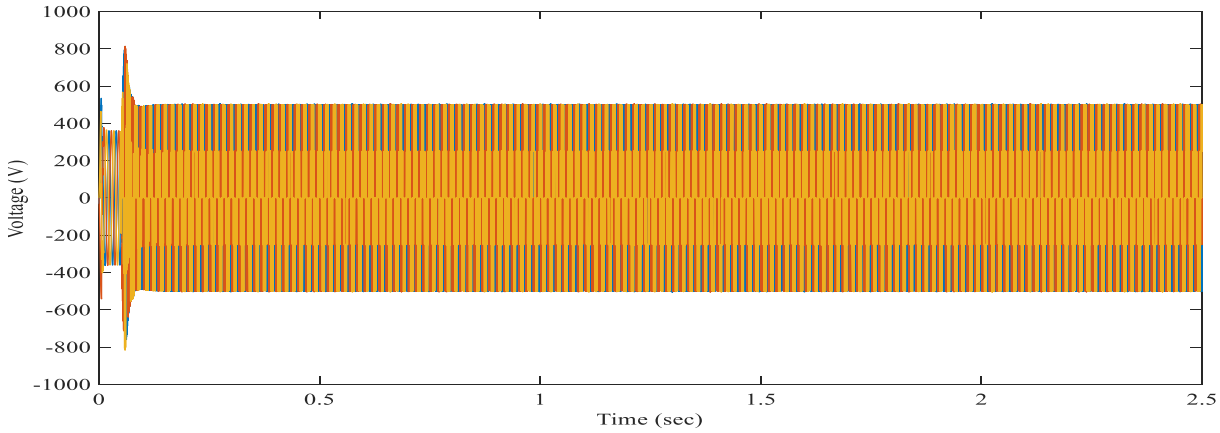

Fig. 11 Voltage of the VSI's output using the PI-HHO controller

It reduces switching power losses by 50% compared to a hard switch. Following passage through an LC filter that displays the voltage level, the square-wave inverter voltage is converted into a three-sinusoidal voltage. Comparing the output voltages to the PI controller without optimization, Fig. 11 demonstrates how the harmonics and ripples have diminished.

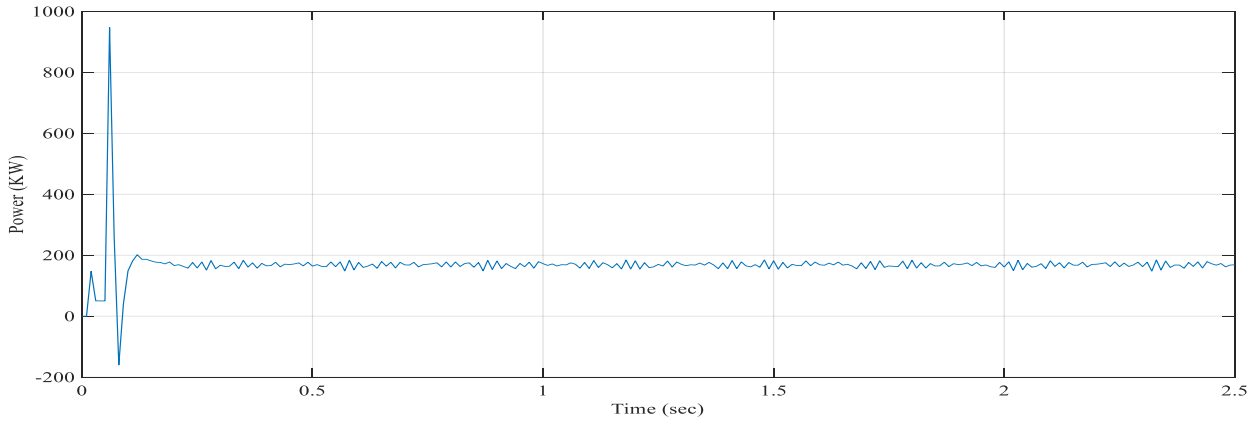

Fig. 12 PI Controller-controlled grid power regulation

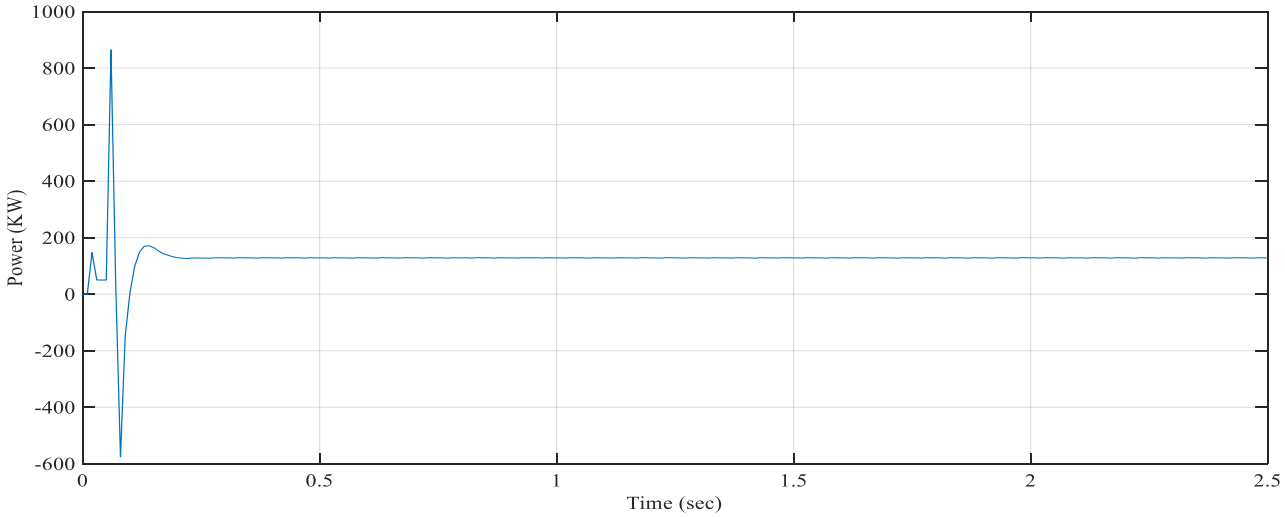

Fig. 13 Grid power regulation using PI Controller HHO

Furthermore, Fig. 12, 13, 14, 15 and 16 show how the grid's-controlled voltage, power, and current are displayed. It is evident from Fig. 13 that the 128kW of power comes from the grid. The efficacy of the proposed system has been improved by using the soft-switching QRBB DC-DC converter.

Optimal gain values can be attained by properly tuning the PI controller by HHO and maintaining the grid parameters under its different operating conditions. The optimal values of HHO optimized PI gain are KP= 0.3, Ki=20 for the vdc regulator and KP=7, Ki=800 for the current regulator.

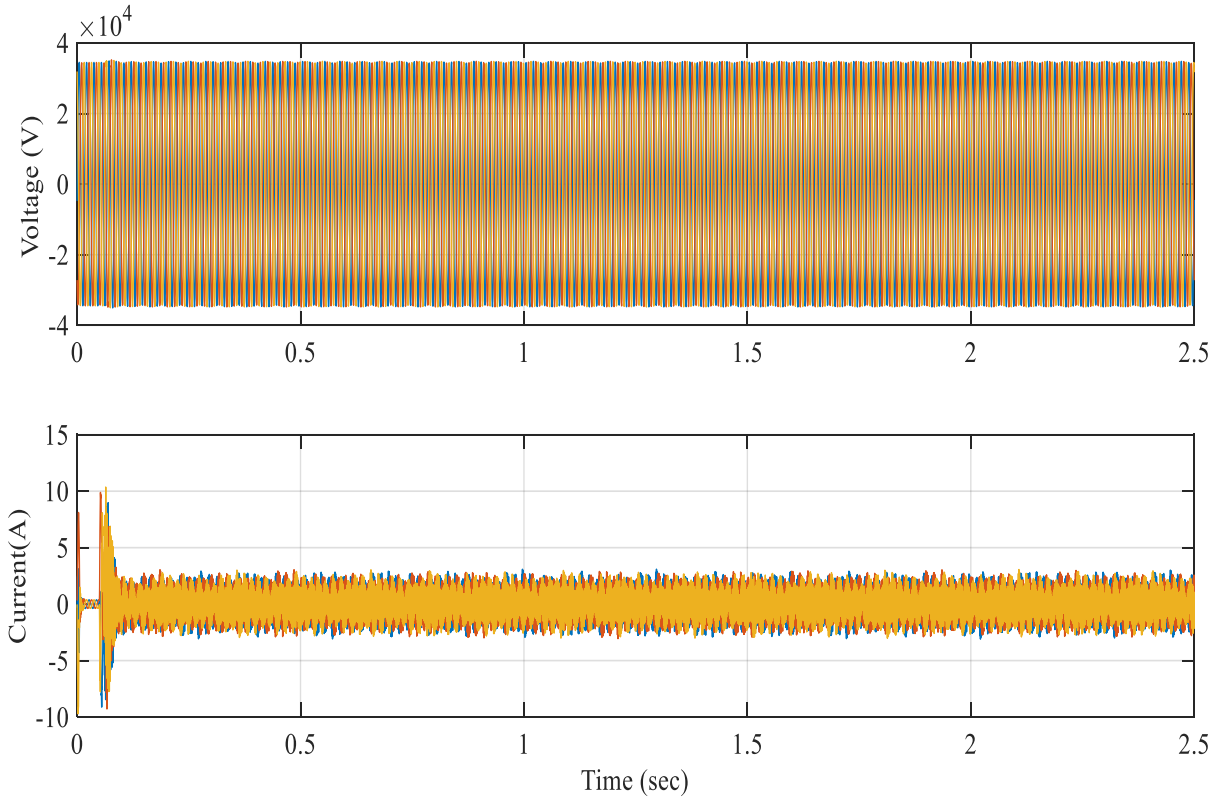

Fig. 14 Grid voltage and current were regulated using a PI Controller

This optimal value manages the system to reduce the drop in voltage fluctuations and maintain the power quality of the grid during different switching modes.

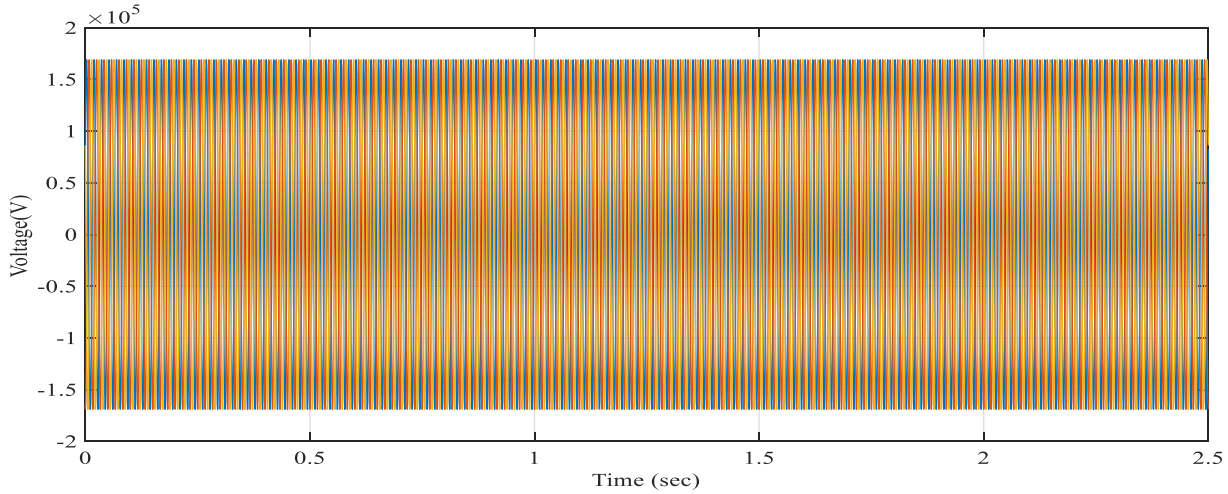

Fig. 15 Controlled grid voltage using PI, the HHO Controller

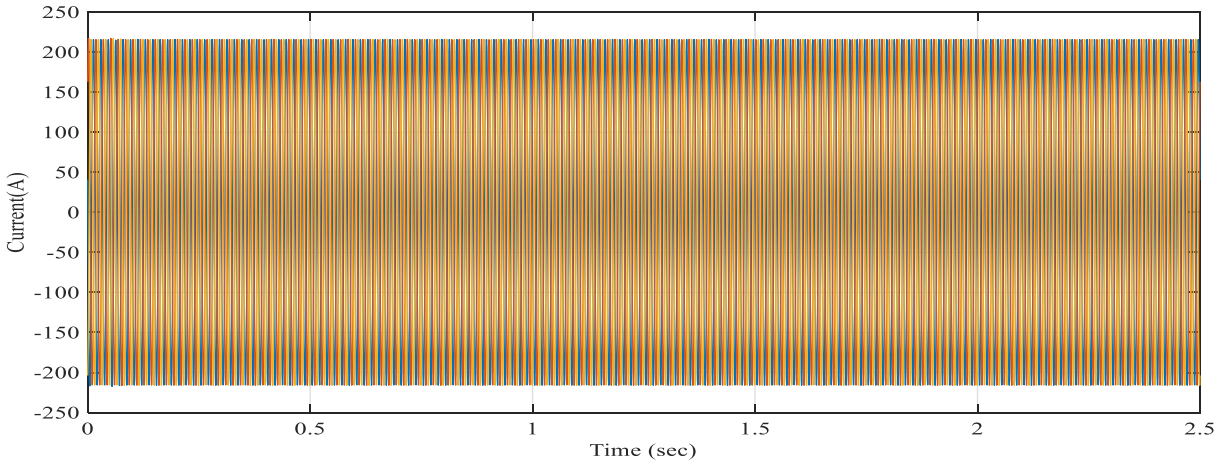

Fig. 16 PI-HHO Controller-controlled grid current

When a soft switching QRBB converter is utilized with a PI-HHO controller as opposed to a traditional PI controller, Grid side waveforms demonstrate that the harmonics have been reduced and the power factor has remained constant. The switching losses in the ZVT PWM converter are considerably reduced. Switching strains and losses in the current and voltage waveforms are also reduced.

4. Conclusion

The switching losses and conduction losses in the converters using grid connected SPV system was removed in this paper using the ZVT–ZCT principle. Based on the simulation results, the total power losses associated with hard switching are higher than those associated with soft switching. During soft switching, the current/voltage remains zero in the switching periods for a finite time, under either ZVT or ZCT conditions. Adding the LC resonant circuit to the Buck-boost converter effectively achieves quasi-resonant soft switching. In addition, the main power circuit's current and voltage stresses are greatly reduced, and the auxiliary components are configured to cope with allowable voltage and current. Soft switching will thereby improve the efficiency and dependability of the PV energy conversion system. In addition, the proposed system with PI controller and HHO-tuned PI is being evaluated. Under the same operating condition and controller configuration, the PI-HHO controller provides a better steady and dynamic state response and delivers quality power to the grid compared to the conventional PI controller. The suggestion of implementing the hardware is still under consideration.

Acknowledgements

The Author, with deep gratitude, would thank the supervisor for his guidance and constant support during this research.

References

[1] S. S. Kumar, A. K. Panda, and T. Ramesh, “A Zvt–Zct Pwm Synchronous Buck Converter with a Simple Passive Auxiliary Circuit for Reduction of Losses and Efficiency Enhancement“, *Ain Shams Engineering Journal*., vol.6, no.2, pp.491-500, 2015.

[2] Mohammed. S. Mohammed, Khaled. M. Al-Awasa, Husssein. D. Al-Majali, "Energy Management and Control in Micro Grid with Hybrid Energy Storage Systems By Using Pi and Flatness Theory," *International Journal of Engineering Trends and Technology*, vol.69, no.11, pp.227-235, 2021, Crossef, Https://Doi.Org/10.14445/22315381/IJETT-V69I11P229.

[3] Khodabandeh, M., Afshari, E. and Amirabadi, M., “A Family of Ćuk, Zeta, and Sepic Based Soft-Switching Dc-Dc Converters,” *IEEE Transactions on Power Electronics*, vol.34, no.10, pp.9503-9519, 2019.

[4] Nourieh, N., Adib, E. and Wheeler, P., Zvt High Step-Up Boost Converter with Wide Input Voltage and Wide Output Power for *Renewable Energy Applications*, 2022.

[5] Yau, Y.T., Hwu, K.I. and Shieh, J.J, “Soft Switching of Non-Isolated Buck-Type Converter with Common-Ground Switch,” *Energies*, vol.14, no.17, pp.5290, 2021.

[6] Mageshwari, S. and Kumar, J.V, “Implementation of Pso Algorithm in Novel Sepic Converter with Pv Fed Source,” in *Interdisciplinary Research in Technology and Management*, Crc Press, pp.160-167, 2021.

[7] S. Jalilzadeh, and M. Pakdel, “A Soft Switched Dc-Dc Boost Converter for Use in Grid Connected Inverters,“ *Journal of Operation and Automation in Power Engineering*, vol.5, no.1, pp.75-82, 2017.

[8] X. Wang, H. Xiao, Z. Wei, and C. Chen, “An Improved Transformerless Photovoltaic Grid-Connected Soft-Switching Inverter,“ *in 14th IEEE Conference on Industrial Electronics and Applications (ICIEA)*, pp.2338-2343, 2019.

[9] Lee, H. J., Kim, and Y. H, "Analysis and Design of A Zvt Resonant Boost Converter Using An Auxiliary Resonant Circuit," *Electronics*, vol.8, no.4, pp.466, 2019.

[10] A. Marrekchi, S. Sallem, and M. B. Kammoun, "A New Soft Switching Algorithm for Active and Reactive Power Control in Three Phase Grid-Connected Pv Plant", *In16th International Multi-Conference on Systems, Signals & Devices* (Ssd), pp.578-582, IEEE, 2019.

[11] U. Khaled, H. Farh, S. Alissa, A. Abanmi, and O. Aldraimli, "Efficient Solution of the Dc-Link Hard Switching Inverter of the Pv System", *Journal of King Saud University-Engineering Sciences*, vol.32, no.7, pp.425-31, 2020.

[12] Appathurai, A., Carol, J. J., Raja, C., Kumar, S. N., Daniel, A. V., Malar, A. J. G., and Krishnamoorthy, S, "A Study on Ecg Signal Characterization and Practical Implementation of Some Ecg Characterization Techniques," *Measurement*, vol.147, pp.106384, 2019.

[13] M. Salem, A. Jusoh, N. R. Idris, H. S. Das, and I. Alhamrouni, "Resonant Power Converters with Respect To Passive Storage (Lc) Elements and Control Techniques–An Overview," *Renewable and Sustainable Energy Reviews*, vol.91, pp.504-20, 2018.

[14] Mr. Anem Apparo, Dr. G. Chandra Sekhar "A Grid Connected Hres Using Seven Level Inverter - A Hybrid Mfo-Rbfnn Technique," *International Journal of Engineering Trends and Technology*, vol.68, no.7, pp.56-68, 2020, Crossef, Https://Doi.Org/ 10.14445/22315381/IJETT-V68I7P209S.

[15] M. S. Ramkumar, A. Amudha, P. Nagaveni, G. Emayavaramban, S. Divyapriya, V. M. Mansoor, M. Sivaramkrishnan, D, and Kavitha, "Analysed Results of Dc-Dc Converters with Softswitching Techinques," *Materials Today: Proceedings*, vol.37, pp.2631-5, 2021.

[16] M. Rezvanyvardom, and A. Mirzaei, "High Gain Configuration of Modified Zvt Sepic-Boost Dc-Dc Converter with Coupled Inductors for Photovoltaic Applications", *Solar Energy*, vol.208, pp.357-67, 2020.

[17] Sivasankari, B., Ahilan, A., Jothin, R., and Malar, A. J. G, "Reliable N Sleep Shuffled Phase Damping Design for Ground Bouncing Noise Mitigation," *Microelectronics Reliability*, vol.88, pp.1316-1321, 2018.

[18] Malar, A. J. G., Kumar, C. A., and Saravanan, A. G, "Iot Based Sustainable Wind Green Energy for Smart Cites Using Fuzzy Logic Based Fractional Order Darwinian Particle Swarm Optimization," *Measurement*, vol.166, pp.108208, 2020.

[19] Ahmad Hamdan Ariffin, Zeittey Karmilla Kaman , "Review on Consumers' Privacy and Economic Value Acceptance in Smart Grid Implementation," *International Journal of Engineering Trends and Technology* , pp.16-20, 2020.

[20] Shenoy, K.L., Nayak, C.G. and Mandi, R.P., "Effect of Partial Shading in Grid Connected Solar Pv System with Fl Controller," *International Journal of Power Electronics and Drive Systems*, vol.12, no.1, pp.431, 2021.

[21] Nimita Gajjar, Tejas Zaveri, Naimish Zaveri, "Low-Cost Implementation of Pv-Statcom for Non-Linear Load Using Stm32f407vg Controller," *International Journal of Engineering Trends and Technology*, vol.69, no.9, pp.212-219, 2021, Crossef, Https://Doi.Org/10.14445/22315381/IJETT-V69I9P225.

[22] Malar, J. G., & Kumar, C. A. Implementation of Mppt Techniques for Wind Energy Conversion System," *Internal Journal of Research and Analytical Reviews*, vol.5, no.3, 2018.

[23] S. Ekinci, B. Hekimoğlu, A. Demirören, and S. Kaya, "Harris Hawks Optimization Approach for Tuning of Fopid Controller in Dc-Dc Buck Converter", *in International Artificial Intelligence and Data Processing Symposium (Idap)*, IEEE, pp.1-9, 2019.

[24] Batarseh, A. Harb, "*Power Electronics*. Springer Nature", 2018.